



This is a repository copy of *Modal decomposition of coupled instabilities: The method of the equivalent nodal forces*.

White Rose Research Online URL for this paper:
<http://eprints.whiterose.ac.uk/147178/>

Version: Accepted Version

Article:

Becque, J., Li, X. and Davison, B. (2019) Modal decomposition of coupled instabilities: The method of the equivalent nodal forces. *Thin-Walled Structures*, 143. 106229. ISSN 0263-8231

<https://doi.org/10.1016/j.tws.2019.106229>

Article available under the terms of the CC-BY-NC-ND licence
(<https://creativecommons.org/licenses/by-nc-nd/4.0/>).

Reuse

This article is distributed under the terms of the Creative Commons Attribution-NonCommercial-NoDerivs (CC BY-NC-ND) licence. This licence only allows you to download this work and share it with others as long as you credit the authors, but you can't change the article in any way or use it commercially. More information and the full terms of the licence here: <https://creativecommons.org/licenses/>

Takedown

If you consider content in White Rose Research Online to be in breach of UK law, please notify us by emailing eprints@whiterose.ac.uk including the URL of the record and the reason for the withdrawal request.



eprints@whiterose.ac.uk
<https://eprints.whiterose.ac.uk/>

MODAL DECOMPOSITION OF COUPLED INSTABILITIES: THE METHOD OF THE EQUIVALENT NODAL FORCES

Jurgen Becque, Xilin Li and Buick Davison

Department of Civil and Structural Engineering, The University of Sheffield

Abstract:

A solution to the 'modal decomposition problem' encountered within the context of the stability analysis of thin-walled structural members is presented. The proposed method achieves decomposition of a randomly deformed shape into a number of constituent modes, which have the physical meaning of the classical local, distortional and global buckling modes, augmented with two additional classes of shear and transverse extension modes. The basis vectors of these five classes are created by defining sets of nodal forces which, when applied to the member in a first order linear elastic problem, generate shapes commensurate with specific mechanical criteria defining the local, distortional, global, shear and transverse extension modes. In a second step the basis vectors of a given class are used to define a constrained stability problem, where the solution is restricted to a linear combination of these basis vectors, in order to obtain the buckled shapes under a given loading. The full set of buckling modes spanning the five classes forms an orthonormal basis of the complete deformation space. Consequently, decomposition can be achieved by projecting the shape which is to be decomposed onto the basis vectors. Two examples are provided to illustrate the method.

Keywords: coupled instabilities, decomposition, buckling modes, local buckling, distortional buckling, global buckling

1. Introduction

Thin-walled structural members have a wide range of applications in aeronautical, nautical, mechanical and structural engineering due to their many advantages, pre-eminently a light weight and an efficient material use. However, due to their limited wall thickness they are susceptible to a range of possible instabilities. In thin-walled columns and beams these instabilities are traditionally categorized in three different classes, namely local, distortional and global (or overall) buckling modes. The distinction between these classes is based on a mechanical description of the buckling modes, but also has a historical context. It is well-known that Euler in 1757 laid the groundwork for the description of the global flexural mode in compressed bar elements. However, a more complete description of column buckling, inclusive of torsional and flexural-torsional modes, did not come along until the 1930's and is credited to the work by Kappus [1], Wagner and Pretschner [2], Bleich and Bleich [3], and Goodier [4]. On the other hand, the description of local buckling finds its origins in the plate theory developed by Saint Venant [5]. The cross-section of a steel structural member can typically be seen as a collection of individual plates connected along their longitudinal edges, which makes it possible to apply classic plate theory to determine the local buckling loads of plate assemblies, provided that appropriate continuity conditions are accounted for at the plate junctions. Early work in this direction was carried out by Lundquist et al. [6], Bleich [7], Chilver [8] and Bulson [9]. Contrary to the global flexural mode, local buckling modes display a stable post-buckling range and a significant amount of post-buckling reserve capacity can be achieved in slender plates or plate assemblies which buckle at stresses well below the yield stress of the material. An empirical equation to predict the ultimate local buckling capacity of plates based on a slenderness parameter was famously proposed by Winter [10, 11] and has been incorporated in all major design standards around the world.

Early understandings of distortional buckling associated the mode with 'stiffener buckling', in which a stiffener bends out synchronously with a plate buckling in a local mode, while increasing the critical stress and prolonging the wavelength. Within the stability analysis of cross-sections this introduces an artificial and eventually untenable distinction between actual plate elements subject to local buckling and other plate elements which merely act as stiffeners. Much of the recognition of distortional buckling as a separate instability, displaying characteristics of both local and global modes, but distinguishing itself from the former by in-plane displacements of some of the constituent plates, can be credited to the work by Hancock [12, 13]. Compared to the local modes, distortional modes typically display much less post-buckling capacity. As an illustrative example Fig.

1 shows the typical cross-sectional deformations associated with local, distortional and global modes in a lipped channel column.

In experimental as well as numerical investigations of thin-walled structural members, it is very frequently observed that local, distortional and global modes do not occur in isolation in their ‘pure’ forms, but appear in combinations, while interacting with each other. These interactions are detrimental in nature and reduce the capacity of the member to below the capacities associated with the individual instabilities. In this respect a distinction is usually made between ‘true interaction’, where buckling modes appear simultaneously at the point of buckling, and ‘secondary bifurcation’, where a second mode appears within the post-buckling range of the first [14]. An attempt can be made to determine the modes participating in a certain deformed shape (obtained experimentally or numerically) by visual inspection. However, this is not always straightforward, especially when the participation of one of the modes is relatively minor. Moreover, to promote a more systematic understanding of coupled instabilities, it is desirable to be able to quantify the contributions of the pure individual modes numerically. The problem of defining and generating the pure buckling modes and subsequently determining the participation of these modes in a random deformed shape is known as the ‘modal decomposition problem’ and it is one this paper aims to provide a solution to.

The solution will be presented within the context of the Finite Strip Method (FSM), although the proposed methodology is more generally applicable and can also be used, for instance, with finite elements. The FSM was originally developed by Przemieniecki [15], Planck and Wittrick [16] and Cheung [17]. Often referred to as the ‘semi-analytical FSM’, the method uses polynomial displacement functions in the transverse direction and continuously differentiable harmonic functions in the longitudinal direction, inspired by theoretical solutions. A discretisation of the member in the longitudinal direction is therefore not required. A brief introduction on the key features of the FSM is provided in Section 2.

Previous studies on modal decomposition have mainly centred around Generalized Beam Theory (GBT). GBT was originally developed by Schardt [18, 19] and can be seen as an extension of the classical theories of bending and torsion to include distortional and local modes. In this extension Vlassov’s assumptions [20] of zero shear strain and zero transverse strain in the mid-plane are maintained. The so-called fundamental equations of GBT, obtained by expressing equilibrium of a member free of external forces, are de-coupled by simultaneously diagonalizing two of the three stiffness matrices. A complete diagonal form of all three stiffness matrices cannot be achieved. However, for open cross-sections this is of minor concern. A complete description of the procedure,

including the additional steps required to obtain the global modes, can be found in [21] and [22]. A significant amount of research work has been devoted to the further development of GBT over the past decades, with the most important contributions being the extension of GBT to closed cross-sections and the addition of shear and transverse extension modes [23-25]. However, it should be emphasized that a GBT analysis results in a set of cross-sectional first order **deformation** modes. GBT modes are not buckling modes, because they are not the solutions of a stability analysis problem.

The ability of GBT to achieve decomposition into a set of deformation modes has inspired Adany and Schafer [26-28] to develop the constrained Finite Strip Method (cFSM). In the cFSM, a number of GBT-based mechanical criteria are used to classify buckling modes into local, distortional, global and 'other' (shear and transverse extension) modes. These criteria are then translated into constraint matrices applied to the shape vectors in the FSM stability eigenvalue problem. The solution of this problem yields a set of buckling modes, which, however, exhibit some shortcomings. Most importantly, the resulting global and distortional modes obey Vlasov's assumptions of zero membrane shear strains and zero membrane transverse strains and are thus idealized modes. Indeed, the FSM has a sufficient number of independent degrees of freedom to account for membrane shear and transverse extension effects in those modes and, consequently, introducing the GBT assumptions into the FSM 'over-constrains' the modes. This is particularly obvious for the cFSM global flexural mode, in which the transverse membrane extensions due to the Poisson's effect are completely constrained, resulting in a critical stress which exceeds the Euler load by a factor $1/(1-\nu^2)$ (where ν is the Poisson's ratio). Moreover, a 'pure' flexural mode in the FSM output would still not be identified by the cFSM as such, but rather as a combination of an idealized 'GBT' flexural mode with added shear and transverse extension modes. The same comments can be made for the distortional modes. As such, the interpretation of the cFSM modes, which are essentially buckling modes since they result from solving a (constrained) stability problem, reverts back to that of deformation modes akin to the GBT framework. This ambiguity, together with the fact that the complete set of cFSM modes, although constituting an independent set of basis vectors of the deformation space, lacks orthogonality, make the cFSM a fundamentally inelegant and uneasy solution to the modal decomposition problem.

Solving the modal decomposition problem, however, is of fundamental importance in order to advance design methods for thin-walled structures, in particular the Direct Strength Method (DSM) [29], which relies on the determination of the individual local, distortional and global elastic buckling stresses. The FSM is commonly used to determine these stresses. However, its application is

hampered by the occurrence of coupled modes in the output and by so-called ‘indistinct minima’ [30]. Both issues can be resolved by modal decomposition.

The objective of this paper is to propose an alternative modal decomposition method which does not suffer from the above-mentioned shortcomings. The proposed method does not rely on GBT principles and allows a more ‘natural’ description of buckling modes, which includes Poisson’s effects and shear deformations. It results in a set of buckling modes which form a completely orthogonal basis of the full deformation space. This facilitates the modal decomposition process, since decomposition can be achieved by simply projecting the deformed shape which is to be decomposed onto the basis vectors.

It should also be noted that two alternative decomposition methods, based however on completely different principles, have already been proposed by the first author and co-workers. The ‘polarization method’ [31] separates deformation modes by either minimizing or maximizing the proportion of plate bending energy in the total strain energy. Karakonstantis and Becque [32] achieved modal decomposition based on a purely mechanical description of the buckling modes. The principles of the method presented in this paper were first presented by the authors in 2016 [33]. Research based on similar principles has since been conducted by others in [34].

2. The finite strip method

For a full and detailed description of the FSM the reader is referred to Cheung and Tham [35]. This paragraph only aims to summarize some of the basic principles.

In the FSM, the member is discretized into a number of longitudinal strips, separated by ‘nodal lines’ (Fig. 2). In what follows, these nodal lines will simply be referred to as ‘nodes’. N is the total number of nodes in the cross-section, which can be subdivided as follows:

- N_m main nodes (Fig. 3), which connect adjacent strips of which the local y -directions are not aligned. The local coordinate system is illustrated in Fig. 2, with the x -axis oriented along a nodal line, the y -axis positioned in the plane of the strip and the z -axis pointed along the normal to the strip. The global X -axis is also parallel to the longitudinal axis of the member, with the global Y - and Z -axes arbitrarily chosen within the plane of the end section. The number of main nodes is pre-determined by the geometry of the section. The external main nodes, located along the free edges of the section, constitute a special case. For an unbranched open section the number of external main nodes $N_{me} = 2$. The remaining N_{mi} main nodes are labelled internal main nodes.

- N_s sub-nodes (or intermediate nodes), which connect two adjacent strips with collinear y-axes. The number of sub-nodes is arbitrary. Sub-nodes can be used to increase the accuracy of the solution.

Each nodal line features four degrees of freedom (Fig. 4): the in-plane y-displacement v , the out-of-plane z-displacement w and the rotation about the x-axis θ , all measured at mid-length along the nodal line, in addition to the (equal and opposite) x-displacements u at the ends of the nodal line. The in-plane (membrane) displacements of a strip contained between adjacent nodal lines i and j are determined by the degrees of freedom u_i and u_j , as well as v_i and v_j . The plate bending deformations within the strip, on the other hand, are determined by w_i , w_j , θ_i and θ_j . In the FSM formulation the theory of small displacements is employed to describe plate bending, resulting in the membrane displacements and the plate bending displacements being completely uncoupled in the local coordinate system. This is a useful characteristic which will be exploited in the decomposition procedure.

In the conventional format of the FSM, developed for members with pinned boundary conditions, the shape functions are sinusoidal in the longitudinal direction for v and w (but co-sinusoidal for u), linear in the transverse direction for u and v , and cubic in the transverse direction for w .

The elastic and geometric stiffness matrices of each strip are formulated in the local coordinate system [35] and subsequently assembled into the global elastic and geometric stiffness matrices \mathbf{K} and \mathbf{G} of the member. The resulting eigenvalue problem has the form:

$$(\mathbf{K} - \lambda \mathbf{G}) \mathbf{v} = \mathbf{0} \tag{1}$$

The eigenvectors \mathbf{v} represent the buckled shapes of the member, while the eigenvalues λ determine the corresponding buckling stresses. The lowest eigenvalue λ_{cr} determines the critical buckling stress. However, the solutions \mathbf{v} may be coupled instabilities.

The computational efficiency of the FSM allows the user, in a very short timeframe, to obtain the so-called ‘signature curve’ of a given cross-section, which plots the critical stress vs. the buckle half-wave length assumed in the longitudinal shape functions. An example is plotted in Fig. 5 in solid black line. Solving the modal decomposition problem in this context consists of: (1) determining the pure (local, distortional, ...) buckling modes, of which the corresponding buckling stresses are also plotted in Fig. 5, and (2) determining the participation of these modes in the FSM output, which is equivalent to expressing the FSM output as a linear combination of the pure modes.

It can easily be proven [31] that the solutions \mathbf{v} of Eq. (1) have the property of orthogonality, both with respect to the matrix \mathbf{K} and the matrix \mathbf{G} :

$$\mathbf{v}_i^T \cdot \mathbf{K} \cdot \mathbf{v}_j = 0 \quad (2)$$

$$\mathbf{v}_i^T \cdot \mathbf{G} \cdot \mathbf{v}_j = 0 \quad (3)$$

where \mathbf{v}_i and \mathbf{v}_j are solutions of Eq. (1) belonging to different eigenvalues λ_i and λ_j .

3. Derivation

Consistent with alternative (GBT-based) decomposition methods [22, 28] the pure buckling modes are categorized into the conventional local, distortional and global modes, augmented with shear and transverse extension modes, which are necessary for the set of buckling modes to span the full deformation space. The subscripts L, D, G, S and TE will be used throughout the remainder of this paper to indicate variables related to these modes, respectively, while the notation \mathbf{d} is used to indicate the pure mode vectors.

If \mathbf{d}_i is a pure buckling mode, fitting into any of the above categories, then we can calculate:

$$\mathbf{K} \cdot \mathbf{d}_i = \mathbf{f}_i \quad (4)$$

Eq. (4) is the first order linear elastic problem corresponding to the stability eigenvalue problem Eq. (1). It shows that there exists a unique set of nodal forces \mathbf{f}_i which, when applied to the member in a linear elastic problem, generates exactly the buckled shape \mathbf{d}_i . While this principle is straightforward, determining the sets of equivalent nodal forces \mathbf{f}_i which can generate the local, distortional, global, shear and extension modes in a given member is anything but obvious. In the following derivation these nodal forces are determined by exploiting some of the mechanical features of the buckling classes, as well as by imposing orthogonality between the modes.

In terms of defining orthogonality, several choices are possible, although orthogonality with respect to the stiffness matrix \mathbf{K} (Eq. 2) is the most obvious one. We therefore define an inner product (using the bracket notation):

$$\langle \mathbf{v} | \mathbf{w} \rangle = \frac{1}{2} \mathbf{v}^T \cdot \mathbf{K} \cdot \mathbf{w} = \frac{1}{2} \mathbf{w}^T \cdot \mathbf{K} \cdot \mathbf{v} \quad (5)$$

Two vectors \mathbf{v} and \mathbf{w} are orthogonal if $\langle \mathbf{v} | \mathbf{w} \rangle = 0$, or yet, using Eq. (4):

$$\mathbf{v}^T \cdot \mathbf{f}_w = \mathbf{w}^T \cdot \mathbf{f}_v = 0 \quad (6)$$

where \mathbf{f}_w is the set of nodal forces generating the deformed shape \mathbf{w} and \mathbf{f}_v are the nodal forces generating the shape \mathbf{v} .

A vector \mathbf{v} is normalized if:

$$\langle \mathbf{v} | \mathbf{v} \rangle = \frac{1}{2} \mathbf{v}^T \cdot \mathbf{K} \cdot \mathbf{v} = 1 \quad (7)$$

The factor of $\frac{1}{2}$ is introduced in Eq. (5) compared to Eq. (2) to give the inner product the physical meaning of a strain energy. Two buckling modes are thus orthogonal if the (alien) work done by the stresses of one mode in the strains of the other mode is zero, or alternatively, according to Eq. (6), if the work done by the equivalent nodal forces of one mode in the displacements of the other mode is zero.

3.1 Local modes

The local buckling modes are most commonly defined as those modes where only out-of-plane displacements (and associated rotations) of the constituent plates take place, with no contributions of the other degrees of freedom. In particular, there are no in-plane transverse or longitudinal membrane displacements. While this definition suffices for our purposes, a few remarks are in order. First, this definition is only possible within the context of small deflection plate theory, in which the plate deflections are uncoupled from the membrane displacements (as is the case in the FSM). Second, this definition becomes somewhat problematic when cross-sections are considered which have rounded transitions from one constituent plate to the other (as practical ‘real-life’ cross-sections always do) and the rounded corner zones are approximated with a number of straight segments. In this case, applying the above definition would pre-empt any rotation of the corner zones. This problem is discussed in [31] and a solution using the ‘polarization method’ is presented. The scope of this paper will be limited to cross-sections with ‘sharp’ corners.

A direct consequence of the above definition is that the corners of a cross-section (coinciding with the internal main nodes as defined in Section 2) necessarily have to remain in place when local buckling occurs. Indeed, any displacement of a main node would inevitably contain a transverse in-plane displacement component in the local coordinate system of at least one of the adjacent plates, since their local normal vectors do not align. Consequently, the local buckling modes can be completely described by a well-defined subset of degrees of freedom:

1. The rotations θ of all nodes.

2. The out-of-plane displacements w of all nodes except the internal main nodes.

The fact that these are the only non-zero degrees of freedom makes it a relatively straightforward exercise to construct a set of basis vectors of the local space. Unit displacements can be imposed, in turn, on each of the above degrees of freedom, while keeping the other degrees of freedom at zero. The basis vectors of the local space \mathbf{v}_L thus consist of a number of $4N \times 1$ vectors containing all zeroes, except at a single location corresponding to one of the above degrees of freedom, where a '1' is encountered. It is easily seen from Eq. (4) that this procedure is equivalent, in terms of nodal forces, to imposing a force (or moment) corresponding to each of the above degrees of freedom, in turn, onto the cross-section, while preventing any other displacement. It also follows from the above definition that the number of local modes is equal to $2N - N_{mi}$.

The basis vectors of the local space \mathbf{v}_L can then be organized as columns in a matrix \mathbf{H}_L (which consequently has dimensions $4N \times 2N - N_{mi}$). The local buckling modes under a given loading are subsequently obtained by solving Eq. (1) while restricting the solutions \mathbf{d}_L to a linear combination of the basis vectors \mathbf{v}_L [26]:

$$\mathbf{d}_L = \mathbf{H}_L \mathbf{a} \quad (8)$$

where \mathbf{a} is a vector of unknown coefficients. This results in the following eigenvalue problem:

$$\left(\mathbf{H}_L^T \mathbf{K} \mathbf{H}_L - \lambda \mathbf{H}_L^T \mathbf{G} \mathbf{H}_L \right) \mathbf{a} = \mathbf{0} \quad (9)$$

After obtaining the eigenvectors \mathbf{a} of Eq. (9) the local modes \mathbf{d}_L follow from Eq. (8). The eigenvalues λ determine the corresponding local buckling stresses.

The lipped channel cross-section with the dimensions shown in Fig. 6 will be used throughout the paper to illustrate the proposed methodology. The cross-section is discretized in the simplest of ways into five strips using six nodes ($N = 6$, $N_{mi} = 4$, $N_{me} = 2$, $N_s = 0$). The eight local modes in uniform compression resulting from Eqs. (8-9) are illustrated in Fig. 7. Fig. 8 illustrates the nodal forces corresponding to the critical local mode (i.e. the one corresponding to the lowest eigenvalue λ in Eq. (9)). The magnitudes of the nodal forces are such that the resulting shape is normalized according to Eq. (7). It is seen that the nodal forces obey translational and rotational equilibrium, which is necessary for the corners of the cross-section to remain in place.

3.2 Distortional modes

In the proposed method the distortional buckling modes are uniquely defined by the following criteria:

- D1. The nodal forces \mathbf{f} which generate the distortional modes ensure translational and rotational equilibrium of the cross-section.
- D2. The components of \mathbf{f} corresponding to the longitudinal in-plane degrees of freedom u are zero. In other words, no longitudinal forces are necessary to generate the distortional modes.
- D3. The transverse membrane stresses are zero.
- D4. The distortional modes are orthogonal to the local modes determined in Section 3.1.

Criterion (D1) reflects the fact that distortional buckling is a cross-sectional instability whereby the structural member overall remains straight. The cross-section distorts but does not undergo any lateral translation or twist. The vector \mathbf{f} , as defined in Eq. (4), contains the nodal forces corresponding to all degrees of freedom.

Criterion (D2) is assumed to apply to all local, distortional, global and transverse extension modes in members with pin-ended boundary conditions. It is, to some extent, a postulate but is inspired by the classical and generalized beam theories where the flexural, torsional and distortional deformation modes can be generated by applying transverse forces only (perpendicular to the axis of the member). This criterion is obviously trivial for the local modes, in which membrane deformations do not participate.

Criterion (D3) equally finds its roots in GBT and classical beam theory. However, in those theories both the transverse membrane strains and the transverse membrane stresses are zero, a premise which is untenable in a more refined formulation. In the development of the cFSM [26] the choice was made to maintain the assumption of zero transverse membrane *strain*, a necessary choice in order to easily relate the longitudinal warping displacements to the cross-sectional displacements. However, when this principle is introduced into the FSM it effectively prevents Poisson's effects from happening, resulting in unnecessary restraint on the distortional and global modes. In our derivation we therefore adopt the more realistic assumption that the transverse membrane *stresses* are zero, an assumption which will be shared between the distortional and global modes (as well as applying in a trivial way to the local modes).

Criterion (D4) combined with criterion (D1) can be seen as a mathematically more precise formulation of the often expressed understanding that the distortional buckling modes are cross-sectional instabilities 'other than the local modes'.

When implementing these conditions mathematically, the cross-sectional equilibrium equations following from criterion (D1) can be written as:

$$\begin{aligned}\sum_{i=1}^N f_Y^i &= 0 \\ \sum_{i=1}^N f_Z^i &= 0 \\ \sum_{i=1}^N (f_Y^i Z_i + f_Z^i Y_i) &= 0\end{aligned}\tag{10}$$

In the above equations, N is the number of nodes, f_Y^i and f_Z^i are the nodal force components in the global Y and Z directions at node i , respectively, and Y_i and Z_i are the global coordinates of node i with respect to an arbitrary chosen origin. Eq. (10) can be summarized in matrix form as:

$$\mathbf{C}_1 \mathbf{f} = 0\tag{11}$$

where \mathbf{C}_1 is a $3 \times 4N$ matrix.

At the same time condition (D2) can be written as:

$$\mathbf{f} = \begin{bmatrix} \mathbf{I} \\ \mathbf{0} \end{bmatrix} \hat{\mathbf{f}} = \mathbf{T} \hat{\mathbf{f}}\tag{12}$$

provided that all the longitudinal end forces are organized at the bottom of the vector \mathbf{f} . The reduced $3N \times 1$ vector $\hat{\mathbf{f}}$ contains all nodal forces, in the same order as \mathbf{f} , with the exception of the longitudinal end forces. Furthermore, \mathbf{I} is the $3N \times 3N$ identity matrix and $\mathbf{0}$ is an $N \times 3N$ matrix containing zeroes. Consequently, \mathbf{T} is a matrix of size $4N \times 3N$.

Somewhat surprisingly, condition (D3) is not immediately straightforward to implement within the context of the FSM. The reason lies in the fact that the transverse membrane stress σ_y is naturally composed of two components:

$$\sigma_y = \frac{E}{1-\nu^2} (\varepsilon_y + \nu \varepsilon_x) = \frac{E}{1-\nu^2} \left(\frac{\partial v}{\partial y} + \nu \frac{\partial u}{\partial x} \right)\tag{13}$$

where E is the elastic modulus and ν is the Poisson's ratio. In the FSM the transverse interpolation function for the y -displacements v is linear, yielding a value of ε_y which is constant in the transverse direction within each strip. On the other hand, the displacements u are constructed using a linear interpolation function in the transverse direction multiplied with a cosinusoidal longitudinal function.

After differentiating u with respect to the longitudinal co-ordinate x , an expression is obtained for ε_x which is still linear in the transverse direction within each strip. Therefore, σ_y as defined by Eq. (13) can never be identically equal to zero. This impasse is solved by enforcing condition (3) 'on average' over the strip width:

$$\bar{\sigma}_y = \frac{E}{1-\nu^2} (\varepsilon_y + \nu \bar{\varepsilon}_x) = 0 \quad (14)$$

with:

$$\varepsilon_y = \frac{\partial v}{\partial y} = \frac{v_2 - v_1}{b} \sin\left(\frac{\pi x}{L}\right) \quad (15)$$

$$\begin{aligned} \bar{\varepsilon}_x &= \frac{\partial \bar{u}}{\partial x} = -\bar{u} \left(\frac{\pi}{L}\right) \sin\left(\frac{\pi x}{L}\right) \\ &= -\left(\frac{u_1 + u_2}{2}\right) \left(\frac{\pi}{L}\right) \sin\left(\frac{\pi x}{L}\right) \end{aligned}$$

In the above equations the subscripts '1' and '2' refer to both nodal lines at the boundaries of the strip and a horizontal bar above a variable indicates an average taken over the strip width. As indicated in Figure 4, b is the width of the strip and L is its length. When expressed in global coordinates, Eq. (14) gives rise to the following set of equations:

$$\begin{aligned} &\frac{(V_{1,i} - V_{2,i}) \cos \alpha_i - (W_{1,i} - W_{2,i}) \sin \alpha_i}{b_i} + \\ &\frac{U_{1,i} + U_{2,i}}{2} \left(\frac{\nu \pi}{L}\right) = 0 \quad i = 1 \dots N_p \end{aligned} \quad (16)$$

where N_p is the number of strips and α_i is the angle measured from the local y -axis of strip i to the global Y -axis according to the right-hand rule. Eq. (16) can be organized in matrix form by placing the coefficients of Eq. (16) in a matrix \mathbf{C}_σ in the positions corresponding to the degrees of freedom organized in \mathbf{d} :

$$\mathbf{C}_\sigma \mathbf{d} = 0 \quad (17)$$

or, when expressed in terms of the nodal forces:

$$\mathbf{C}_\sigma \mathbf{d} = \mathbf{C}_\sigma \mathbf{K}^{-1} \mathbf{f} = \mathbf{C}_2 \mathbf{f} = 0 \quad (18)$$

Finally, orthogonality with respect to the local modes previously determined in Section 3.1 (condition D4) requires:

$$\mathbf{H}_L^T \mathbf{K} \mathbf{d} = \mathbf{0} \quad (19)$$

or:

$$\mathbf{H}_L^T \mathbf{f} = \mathbf{0} \quad (20)$$

A practical consequence of this orthogonality condition is that the nodal forces corresponding to the subset of degrees of freedom which define the local modes (Section 3.1) are necessarily zero in the distortional modes. Indeed, the matrix \mathbf{H}_L^T contains the basis vectors of the local space, obtained by imposing a unit displacement on a particular degree of freedom (either a rotation or an out-of-plane displacement of a sub-node or external main node) while keeping the other degrees of freedom at zero. Taking also criterion (D2) into account, the only potentially non-zero components of the equivalent nodal forces \mathbf{f} which generate the distortional modes are thus the Y and Z force components at the internal main nodes and the forces corresponding to the in-plane transverse displacements at all nodes.

Combining Eqs. (11), (12), (18) and (20), the equivalent forces \mathbf{f} generating the distortional modes can be obtained from:

$$\begin{bmatrix} \mathbf{C}_1 \\ \mathbf{C}_2 \\ \mathbf{H}_L^T \end{bmatrix} \mathbf{T} \hat{\mathbf{f}} = \mathbf{C}_D \hat{\mathbf{f}} = \mathbf{0} \quad (21)$$

The matrix \mathbf{C}_D has dimensions $(2N - N_{mi} + N_p + 3) \times 3N$. Eq. (21) shows that the forces generating the distortional modes can be obtained as the kernel (or null space) of the matrix \mathbf{C}_D . In MatLab [36], this can be achieved with the command:

$$\hat{\mathbf{F}}_D = \text{null}(\mathbf{C}_D) \quad (22)$$

The matrix $\hat{\mathbf{F}}_D$ then contains a number of linearly independent column vectors equal to the dimension of the null space. For an open, unbranched cross-section (for which $N_{mi} = N_m - 2$ and $N_p =$

$N - 1$) the number of column vectors in $\hat{\mathbf{F}}_D$ is equal to $N_{mi} - 2$. For a single-cell closed section ($N_{mi} = N_m$ and $N_p = N$) the number of column vectors is $N_m - 3$. For both types of cross-sections the rows of the matrix \mathbf{C}_D are all linearly independent. However, this is not always the case. An example to the contrary is given in Fig. 9. In this cross-section a transverse membrane stress in one plate element (and the associated contraction or expansion of the plate) cannot be imposed without introducing transverse stresses in some of the other plates. Therefore, the conditions of zero transverse stress Eqs. (16), when combined with the remaining criteria (in particular Eqs. 12), do not lead to completely independent rows in the matrix \mathbf{C}_D . This leads to an increase in the dimension of the null space and, consequently, the number of distortional modes. A related issue has been pointed out in the context of GBT by Gonçalves et al. [24], who have provided a more detailed discussion on how to determine the number of distortional, transverse extension and shear modes. However, in the here proposed method the number of distortional modes follows automatically from the numerical process of determining the null space of \mathbf{C}_D (Eq. 22) and the subtleties and exceptions discussed above can conveniently be disregarded by the user. The fact that the proposed method is generally applicable to cross-sections of various geometries without modification is one of its key strengths.

Solving Eq. (22) allows us to calculate:

$$\mathbf{F}_D = \mathbf{T}\hat{\mathbf{F}}_D \quad (23)$$

and, subsequently:

$$\mathbf{H}_D = \mathbf{K}^{-1}\mathbf{F}_D \quad (24)$$

The matrix \mathbf{H}_D then contains a set of basis vectors of the distortional space. These basis vectors are used to formulate a constrained eigenvalue problem similar to Eq. (9):

$$\left(\mathbf{H}_D^T \mathbf{K} \mathbf{H}_D - \lambda \mathbf{H}_D^T \mathbf{G} \mathbf{H}_D\right) \mathbf{a} = 0 \quad (25)$$

with:

$$\mathbf{d}_D = \mathbf{H}_D \mathbf{a} \quad (26)$$

This yields the distortional modes \mathbf{d}_D and the associated distortional buckling stresses λ under a given loading.

For the case of the lipped channel pictured in Figure 6, the number of distortional modes is two. This results from the fact that the total number of degrees of freedom (and thus the number of

components in \mathbf{f} is $4 \times 6 = 24$. Condition (D1), imposing cross-sectional equilibrium of the nodal forces, results in the three Eqs. (10), while conditions (D2) and (D3) result in six and five equations, respectively. Finally, orthogonality with respect to the local modes determined in Section 3.1 (condition D4) yields eight more equations. The number of distortional modes is thus: $24 - (3 + 5 + 6 + 8) = 2$. These modes, together with the nodal forces which generate them, are illustrated in Figure 10. It is seen that the forces corresponding to the subset of degrees of freedom associated with the local modes (as described in Section 3.1) are indeed all zero. In particular, the moments at all nodes, as well as the out-of-plane forces at the external main nodes, are zero. The forces are in translational and rotational equilibrium, as required. It is noted that the forces in Fig. 10 have magnitudes which produce a normalized deformation vector according to Eq. (7).

3.3 Global modes

The global modes distinguish themselves from the distortional modes by the fact that condition (D1) of Section 3.2, requiring cross-sectional equilibrium of the nodal forces, is lifted. Thus, the global modes are characterized as follows:

- G1. No longitudinal end forces are necessary to generate the global modes. The components of \mathbf{f} corresponding to the longitudinal in-plane degrees of freedom u are zero.
- G2. The transverse membrane stresses are zero.
- G3. The global modes are orthogonal to the local and distortional modes previously obtained in Sections 3.1 and 3.2, respectively.

Mathematically this can be expressed as:

$$\begin{bmatrix} \mathbf{C}_2 \\ \mathbf{H}_L^T \\ \mathbf{H}_D^T \end{bmatrix} \mathbf{f} = \begin{bmatrix} \mathbf{C}_2 \\ \mathbf{H}_L^T \\ \mathbf{H}_D^T \end{bmatrix} \mathbf{T} \hat{\mathbf{f}} = \mathbf{C}_G \hat{\mathbf{f}} = \mathbf{0} \quad (27)$$

We then successively calculate:

$$\hat{\mathbf{F}}_G = \text{null}(\mathbf{C}_G) \quad (28)$$

$$\mathbf{F}_G = \mathbf{T} \hat{\mathbf{F}}_G \quad (29)$$

$$\mathbf{H}_G = \mathbf{K}^{-1} \mathbf{F}_G \quad (30)$$

The matrix \mathbf{H}_G then contains, as its columns, a set of basis vectors of the global space. The number of global modes is always equal to three. The matrix \mathbf{H}_G can be used to formulate a constrained eigenvalue problem, similar to Eqs. (9) and (25), to determine the global buckling modes under a given loading determined by the matrix \mathbf{G} :

$$\left(\mathbf{H}_G^T \mathbf{K} \mathbf{H}_G - \lambda \mathbf{H}_G^T \mathbf{G} \mathbf{H}_G \right) \mathbf{a} = \mathbf{0} \quad (31)$$

with:

$$\mathbf{d}_G = \mathbf{H}_G \mathbf{a} \quad (32)$$

This yields the global modes \mathbf{d}_G , while the associated global buckling stresses are determined by the eigenvalues λ . The three global modes of the channel pictured in Figure 6 under uniform compression, together with their nodal forces, are shown in Figure 11. The shapes have been normalized according to Eq. (7).

3.4 Transverse extension and shear modes

The transverse extension modes are found by lifting the requirement of zero transverse stress. They are thus obtained from the following two statements:

TE1. No longitudinal end forces are necessary to generate the transverse extension modes.

TE2. The transverse extension modes are orthogonal to the local, distortional and global modes previously obtained in Sections 3.1 - 3.3.

Mathematically this results in the following system of equations:

$$\begin{bmatrix} \mathbf{H}_L^T \\ \mathbf{H}_D^T \\ \mathbf{H}_G^T \end{bmatrix} \mathbf{f} = \begin{bmatrix} \mathbf{H}_L^T \\ \mathbf{H}_D^T \\ \mathbf{H}_G^T \end{bmatrix} \mathbf{T} \hat{\mathbf{f}} = \mathbf{C}_{TE} \hat{\mathbf{f}} = \mathbf{0} \quad (33)$$

The solution is found from:

$$\hat{\mathbf{F}}_{TE} = \text{null}(\mathbf{C}_{TE}) \quad (34)$$

and, subsequently:

$$\mathbf{F}_{TE} = \mathbf{T} \hat{\mathbf{F}}_{TE} \quad (35)$$

$$\mathbf{H}_{TE} = \mathbf{K}^{-1} \mathbf{F}_{TE} \quad (36)$$

The columns of the matrix \mathbf{H}_{TE} then constitute a set of basis vectors of the transverse extension space. By restricting the solutions of Eq. (1) to a linear combination of these basis vectors, in a similar fashion to Eqs. (9), (25) and (31), the transverse extension modes under a given loading encoded in the matrix \mathbf{G} can be obtained. The transverse extension modes of the channel in Fig. 6 are pictured in Figure 12. The equivalent nodal forces associated with the critical transverse extension mode are pictured in Figure 13. Not surprisingly, they consist of equal and opposite forces which compress/extend one of the strips.

Finally, the shear modes are obtained from orthogonality with all previously obtained modes:

$$\begin{bmatrix} \mathbf{H}_L^T \\ \mathbf{H}_D^T \\ \mathbf{H}_G^T \\ \mathbf{H}_{TE}^T \end{bmatrix} \mathbf{f} = \mathbf{C}_S \mathbf{f} = \mathbf{0} \quad (37)$$

$$\mathbf{F}_S = \text{null}(\mathbf{C}_S) \quad (38)$$

$$\mathbf{H}_S = \mathbf{K}^{-1} \mathbf{F}_S \quad (39)$$

This allows the shear modes \mathbf{d}_S under a given loading to be determined by constraining the solutions of Eq. (1) to a linear combination of the basis vectors of the shear space contained in \mathbf{H}_S . The resulting shear modes are shown in Figure 14 for the channel pictured in Figure 6. As an example, the nodal forces required to generate one of shear mode are also shown in Figure 15. It is seen that longitudinal end forces as well as transverse forces perpendicular to the member axis are needed to generate these modes. Moreover, cross-sectional equilibrium is no longer satisfied. Rather, the longitudinal end forces tend to cause bending and/or torsion of the member, which has to be counteracted by the transverse forces at mid-length. The transverse extension modes, on the other hand, do satisfy cross-sectional equilibrium. This follows from the fact that the transverse extension modes do not have any longitudinal end forces associated with them, while they have to satisfy orthogonality with the global modes, i.e. the cross-sectional forces cannot generate any work when the cross-section undergoes a translation or rotation.

4. Modal decomposition

The set of $4N$ vectors \mathbf{d} , consisting of the pure local, distortional, global, transverse extension and shear modes, \mathbf{d}_L , \mathbf{d}_D , \mathbf{d}_G , \mathbf{d}_{TE} and \mathbf{d}_S , as determined in Section 3, when normalized according to Eq. (7), form an orthonormal basis of the complete deformation space:

$$\langle \mathbf{d}_i / \mathbf{d}_j \rangle = 0 \quad \forall i \neq j \quad i, j = 1 \dots 4N \quad (40)$$

$$\langle \mathbf{d}_i / \mathbf{d}_i \rangle = 1 \quad \forall i \quad (41)$$

Eq. (40) is a consequence of the fact that the different classes of modes have been constructed with mutual orthogonality as a requirement, while within each class the vectors \mathbf{d} are a solution of a constrained eigenvalue problem with the structure of Eqs. (9, 25, 31) and are thus orthogonal with respect to both \mathbf{K} and \mathbf{G} .

This means that any random displacement vector, and in particular any vector \mathbf{v} belonging to the FSM output resulting from Eq. (1), can be written as a linear combination of the vectors \mathbf{d} :

$$\mathbf{v} = \sum_{m=1}^{4N} c_m \mathbf{d}_m \quad (42)$$

Each coefficient c_i in Eq. (42) can be determined by taking the inner product of both sides of the equation with \mathbf{d}_i and using the properties established in Eqs. (40-41):

$$c_i = \langle \mathbf{v} / \mathbf{d}_i \rangle \quad (43)$$

In other words, the coefficients c_i are obtained by projecting \mathbf{v} onto the basis vectors \mathbf{d}_i using the inner product.

When \mathbf{v} is normalized using Eq. (10), the coefficients c_m have the following property:

$$\langle \mathbf{v} / \mathbf{v} \rangle = \frac{1}{2} \left(\sum_{p=1}^{4N} c_p \mathbf{d}_p^T \right) \mathbf{K} \left(\sum_{q=1}^{4N} c_q \mathbf{d}_q \right)$$

$$= \sum_{m=1}^{4N} c_m^2 = 1 \quad (44)$$

The relative participation of a certain class of modes M ($M = L, D, G, TE$ or S) in the total elastic strain energy is then given by:

$$p_M = \frac{\frac{1}{2} \left(\sum_M c_p \mathbf{d}_p^T \right) \mathbf{K} \left(\sum_M c_q \mathbf{d}_q \right)}{\frac{1}{2} \mathbf{v}^T \mathbf{K} \mathbf{v}} = \sum_M c_m^2 \quad (45)$$

where the summation is carried out over all vectors of that class.

Figure 16 shows the conventional FSM output for the lipped channel in Figure 6, as well as the curves for the critical (pure) local, distortional and global modes. The participation of the L, D and G classes of modes in the total elastic energy of the FSM output is also shown. The S and TE modes did not noticeably contribute.

5. Additional example

To illustrate that the proposed method is not restricted to open cross-sections, but universally valid to any cross-section type, the double-cell cross-section pictured in Figure 17 is considered. The cross-section is assumed to be subject to uniform compression and is discretized using six nodes: $N = N_m = N_{mi} = 6$. The subset of degrees of freedom defining the local modes is comprised in this case of the six nodal rotations, resulting in six local modes. The number of distortional modes is two, since this is the difference between 24 (the number of degrees of freedom) and 22 (the number of conditions imposed by criteria D1-D4). Criterion D1 results in three equilibrium conditions, while D2, D3 and D4 provide six, seven and six conditions, respectively. One point-symmetric distortional mode and one distortional mode symmetric about the vertical axis of the cross-section were obtained. All pure modes are shown in Figure 18. Using these modes the FSM output was decomposed into its constituents using the method in Section 4 and the results are shown in Figure 19. Once again, the shear and transverse extension modes did not noticeably contribute.

It is noted that the GBT and the cFSM always generate an 'axial mode' as part of their output. This mode displays uniform axial strains within each cross-section, is shear-free and is usually categorized as a special case of the global modes. A similar mode can be seen in Figure 18 (second shear mode

from the left). However, due to the Poisson's effect which occurs along the column length, but is restrained at the column ends, this mode is not entirely shear-free.

As a general comment on the proposed method, it follows from the above derivation that the equivalent nodal forces (and thus the modal shapes) are dependent on the half-wavelength L . This implies, for instance, that the global flexural mode will slightly change shape for increasing values of L . This is consistent with the underlying fundamentals of the method, in particular the fact that Vlasov's assumptions are no longer adhered to and that, consequently, the global flexural mode will exhibit a minor amount of shear. These shear deformations will naturally become more significant for shorter values of L . This is one of the features which set the method apart from GBT and the cFSM. However, with the exception of very short wavelengths the dependence of the modal shape on L is typically very minor.

6. Application in shell finite element analysis

The above procedure can be employed within the context of shell finite element (FE) analysis, for instance to generate initial imperfections for a member with simply supported boundary conditions in the shape of the pure local, distortional or global modes. In order to achieve this, the isolated nodal forces calculated in Section 3 need to be expanded into sinusoidally distributed line loads along the length of the member. The wavelength of this load pattern is the wavelength corresponding to the minimum of the FSM curve for that specific individual mode (which might have to be slightly adjusted to fit an integer number of half-waves within the length of the member), while the amplitude of the loads equals the magnitude of the nodal forces calculated according to Section 3 for that wavelength. This is illustrated in Figure 20 for one particular force belonging to the set of forces generating the distortional mode in a lipped channel. It is clear that the discretization in the transverse direction needs to be compatible in both the FSM model and the FE model. These sinusoidal line loads are applied to the FE model in a first order linear elastic analysis. The differential equations of the classical theories of beams and plates, as well as the GBT equations then indicate a resulting sinusoidally deformed shape with the same half-wavelength, which is consequently the desired buckled shape. Figure 21 illustrates the critical distortional mode in a lipped channel which was thus generated. The whole procedure, including the FSM-based calculations of Section 3, was automated in a Python script run in ABAQUS [37].

The buckling modes which are thus obtained can be scaled and used as initial imperfections in a non-linear FE analysis. Guidance on how to select appropriate imperfection amplitudes is available in literature (e.g. [38, 39]).

The sinusoidal line loads associated with a certain mode can also be used to determine the contribution of that mode in a random first order deformed FE shape (as expressed by the coefficient c_i in Eq. 43). Indeed, the contribution of the mode in the total strain energy is obtained as the total sum of all products of the nodal forces with the corresponding displacements of the random shape.

It is noted that an alternative GBT-based decomposition method within the context of shell FE analysis has been proposed by Nedelcu and Cucu [40].

7. Conclusions

The contribution of this paper lies in the presentation of a novel method to achieve modal decomposition of a randomly deformed shape of a structural member into the contributions of a set of ‘pure’ individual buckling modes. In most applications this random shape will be a coupled instability and the modal decomposition will serve to quantify the participation of various modes in the phenomenon in order to deepen our understanding, but modal decomposition can also be applied, for instance, to initial imperfections. The pure buckling modes are categorized as the classical local, distortional, and global modes, augmented with transverse extension and shear modes. In a first step the basis vectors of the various classes of pure modes are generated by applying specific sets of nodal forces to a first order linear elastic model of the member. These nodal forces are obtained by mathematically implementing a set of mechanical criteria which determine each class of buckling modes. These criteria are schematically represented in Figure 22. The local, distortional and global modes all share the zero transverse stress criterion. The distortional and global modes are distinguished by the fact that only the former obey cross-sectional equilibrium of the nodal forces. The transverse extension modes also satisfy this equilibrium, while the shear modes in general do not. The shear modes are also the only modes with non-zero longitudinal end forces. In addition, orthogonality (defined based on zero alien work) is enforced between the various classes. Once the basis vectors of a certain class have been determined, the solution of the general stability eigenvalue problem can be constrained to a linear combination of those basis vectors, yielding the buckling modes belonging to that class and corresponding to a given loading.

The full set of local, distortional, global, transverse extension and shear modes form an orthonormal basis of the complete deformation space. As a beneficial result of this property decomposition can

simply be achieved by projecting the deformed shape which is to be decomposed onto these basis vectors.

Unlike previously proposed decomposition methods (in particular GBT and the cFSM) the method is universally applicable without modification to any cross-sectional shape, irrespective of whether this shape is open, closed, open with closed parts, branched or unbranched. Naturally occurring Poisson's effects and shear effects are accounted for in the method. However, this also implies that the pure buckling modes have a minor dependence on the buckle half-wavelength and the GBT view that the buckling modes are fully characterized by their cross-sectional shape and are independent of the half-wave length is no longer valid.

A number of examples have been provided to illustrate the method.

References

- [1] Kappus, R. (1937) "Drillknicken zentrisch gedruckter Stäbe mit offenem Profil im elastischen Bereich." *Luftfahrtforschung*, 14 (9), 444-457 (translated into *NACA Technical Memorandum No. 851* (1938)).
- [2] Wagner, H., and Pretschner, W. (1936). *Luftfahrtforschung*, 11, 174-180 (translated into *NACA Technical Memorandum No. 784*).
- [3] Bleich, H., and Bleich, F. (1936). "Biegung, Drillung und Knickung von Stäben aus Dünnen Wänden." Vorbericht zum 2. Kongress der Internationalen Vereinigung für Brücken- und Hochbau. Verlag Ernst & Sohn, Berlin.
- [4] Goodier, J.N. (1942). "Flexural-Torsional Buckling of Bars of Open Section." *Cornell University Engineering Experiment Station Bulletin*, 28, 16p.
- [5] Saint-Venant, M. (1883). "Discussion en Théorie de l'Elasticité des Corps Solides.", by Clebsch, 704.
- [6] Lundquist, E.E., Stowell, E.Z., and Schuette, E.H. (1943). "Principles of Moment Distribution Applied to Stability of Structures Composed of Bars or Plates." *NACA, Report 809*.
- [7] Bleich, F. (1952). *Buckling Strength of Metal Structures*, McGraw-Hill, New York.

- [8] Chilver, A.H. (1953). "A Generalized Approach to the Local Instability of Certain Thin-Walled Struts." *Aeronautical Quarterly*, 4, 245-260.
- [9] Bulson, P.S. (1970). *Stability of Flat Plates*, Chatto and Windus, London.
- [10] Winter, G.. (1940). "Strength Distribution in and Equivalent Width of Flanges of Wide, Thin-Walled Steel Beams." *NACA Technical Note 784*.
- [11] Winter, G. (1970). *Commentary on the 1968 Edition of the Specification for the Design of Cold-Formed Steel Structural Members*, American Iron and Steel Institute, New York, USA.
- [12] Hancock, G. J. (1978). "Local, distortional and lateral buckling of I-beams." *Journal of the Structural Division*, ASCE, Vol. 104, ST11, pp. 1787-1798.
- [13] Hancock, G. J. (1985). "Distortional buckling of steel storage rack columns." *Journal of Structural Engineering* – ASCE, 111 (12), pp. 2770-2783.
- [14] Camotim, D., Dinis, P.B., Martins, A.D., Young, B. (2018), "Review: Interactive behaviour, failure and DSM design of cold-formed steel members prone to distortional buckling." *Thin-Walled Structures*, 128, 12-42.
- [15] Przemieniecki, J.S. (1973), "Finite Element Structural Analysis of Local Instability." *AIAA*, 11(1), 33-39.
- [16] Plank, R.J., and Wittrick, W.H. (1974). "Buckling under Combined Loading of Thin, Flat-Walled Structures by a Complex Finite Strip Method." *International Journal for Numerical Methods in Engineering*, 8 (2), 323-339.
- [17] Cheung, Y.K. (1976). *Finite Strip Method in Structural Analysis*, Pergamon Press, New York.
- [18] Schardt, R. (1989). *Verallgemeinerte technische biegetheorie* (Generalised beam theory), Springer Verlag, Berlin, Heidelberg.
- [19] Schardt, R. (1994). "Generalized Beam Theory – An Adequate Method for Coupled Stability Problems." *Thin-Walled Structures*, 19(2-4), 161-180.

- [20] Vlasov, W.S. (1958). *Allgemeine Schalentheorie und ihre Anwendung in der Technik*. Akademie Verlag, Berlin.
- [21] Silvestre, N., and Camotim, D. (2002). "First-order generalized beam theory for arbitrary orthotropic materials." *Thin-Walled Structures*, 40, 755–789.
- [22] Bebiano, R., Silvestre, N., and Camotim, D. (2008). *GBTUL 1.0 β - Buckling and vibration analysis of thin-walled members – GBT theoretical background*. Department of Civil Engineering and Architecture, DECivil/IST, Technical University of Lisbon, Portugal.
- [23] Gonçalves, R., Dinis, P.B., and Camotim, D. (2009). "GBT formulation to analyse the first-order and buckling behaviour of thin-walled members with arbitrary cross-sections." *Thin-Walled Structures*, 47(5), 583-600.
- [24] Gonçalves, R., Bebiano, R., and Camotim, D. (2014). "On the shear deformation modes in the framework of Generalized Beam Theory." *Thin-Walled Structures*, 84, 325-334.
- [25] Simão, P., and Simões da Silva, L. (2004). "A unified energy formulation for the stability analysis of open and closed thin-walled members in the framework of the generalized beam theory." *Thin-Walled Structures*, 42, 1495-1517.
- [26] Adany, S., and Schafer, B. W. (2006). Buckling mode decomposition of single-branched open cross-section members via finite strip method: Derivation. *Thin Walled Structures*, 44(5), 563-584.
- [27] Adany, S., and Schafer, B. W. (2006). Buckling mode decomposition of single-branched open cross-section members via finite strip method: Application and Examples. *Thin Walled Structures*, 44(5), 585-600.
- [28] Adany, S., and Schafer, B. W. (2008). A full modal decomposition of thin-walled, single-branched open cross-section members via the constrained finite strip method. *Journal of Constructional Steel Research*, 64(1), 12-29.

- [29] Schafer, B.W., and Peköz, T. (1998). "Direct Strength Prediction of Cold-Formed Steel Members using Numerical Elastic Buckling Solutions." *Proceedings of the 14th International Specialty Conference on Cold-Formed Steel Structures*, St. Louis, Missouri, 69-76.
- [30] Schafer, B. W. (2008). "Review: The Direct Strength Method of cold-formed steel design." *Journal of Constructional Steel Research*, 64(7-8), 766-778.
- [31] Becque, J., and Li, X. (2015). "A new approach to modal decomposition of buckled shapes." *Structures*, 4, 2-12.
- [32] Karakostas, V., and Becque, J. (2014). "Modal classification and decomposition of instabilities in thin-walled structural members." *Proceedings of the 7th International Conference on Thin-Walled Structures, ICTWS 2014*, Busan, Korea.
- [33] Becque, J., and Li, X. (2016). "Modal decomposition of buckled shapes: the method of the equivalent forces." 6th International Conference on Structural Engineering, Mechanics and Computation (SEMC 2016), 5-7 Sep 2016, Cape Town, South Africa; *Insights and Innovations in Structural Engineering, Mechanics and Computation*, ed. Zingoni, A., CRC Press.
- [34] Jin, S., Gan, D., Chen, H., Cheng, R., and Zhou, X. (2018). "A force-based method for identifying the deformation modes of thin-walled members." *Thin-Walled Structures*, 129, 473-487.
- [35] Cheung, Y.K., and Tham, L.G. (1998). *Finite Strip Method*. CRC Press, Boca Raton, USA.
- [36] Mathworks Inc. (2011), Matlab R2011a, Natick, MA, USA.
- [37] ABAQUS (2014). *ABAQUS/CAE User's Guide, v6.14*, Pawtucket, USA.
- [38] Schafer, B.W., and Peköz, T. (1998). "Computational modeling of cold-formed steel: characterizing geometric imperfections and residual stresses", *Journal of Constructional Steel Research*, 47, 193-210.

- [39] Bonada, J., Casafont, M., and Roure, F. (2012). "Selection of the initial geometrical imperfection in nonlinear FE analysis of cold-formed steel rack sections." *Thin-Walled Structures*, 51, pp. 99-111.
- [40] Nedelcu, M., and Cucu, H.L. (2014). "Buckling modes identification from FEA of thin-walled members using only GBT cross-sectional deformation modes." *Thin-Walled Structures*, 81, pp. 150-158.

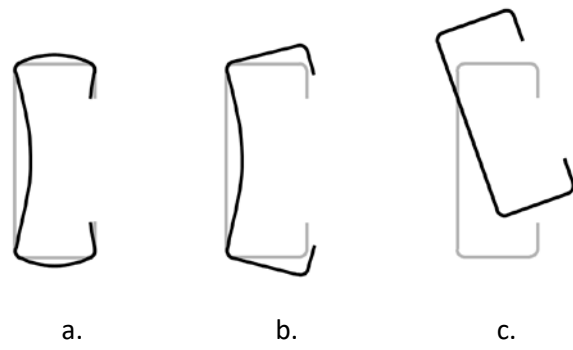


Figure 1: Buckling modes of a lipped channel: a. local, b. distortional, and c. global modes

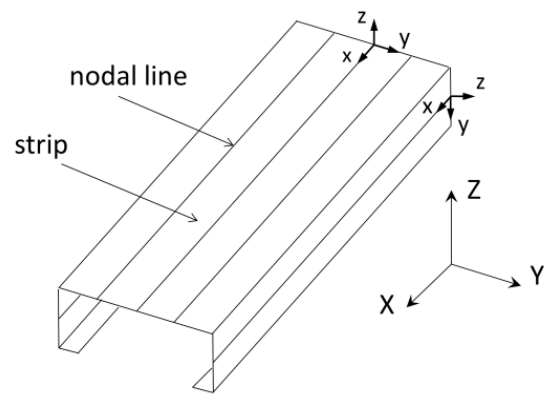


Figure 2: Discretization into strips

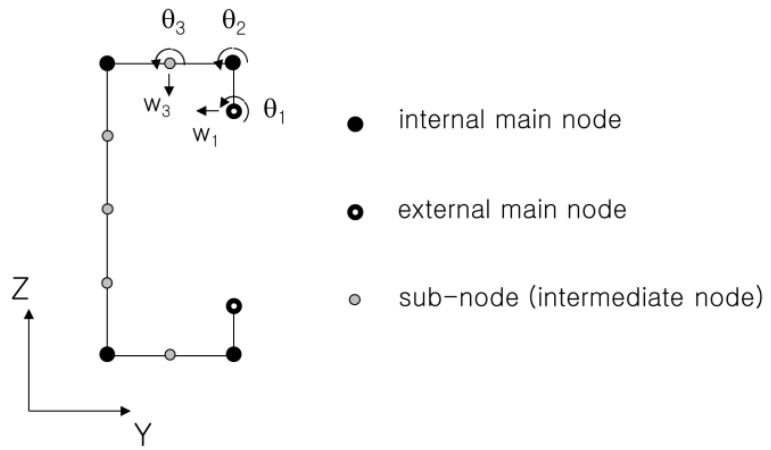


Figure 3: Main nodes and sub-nodes

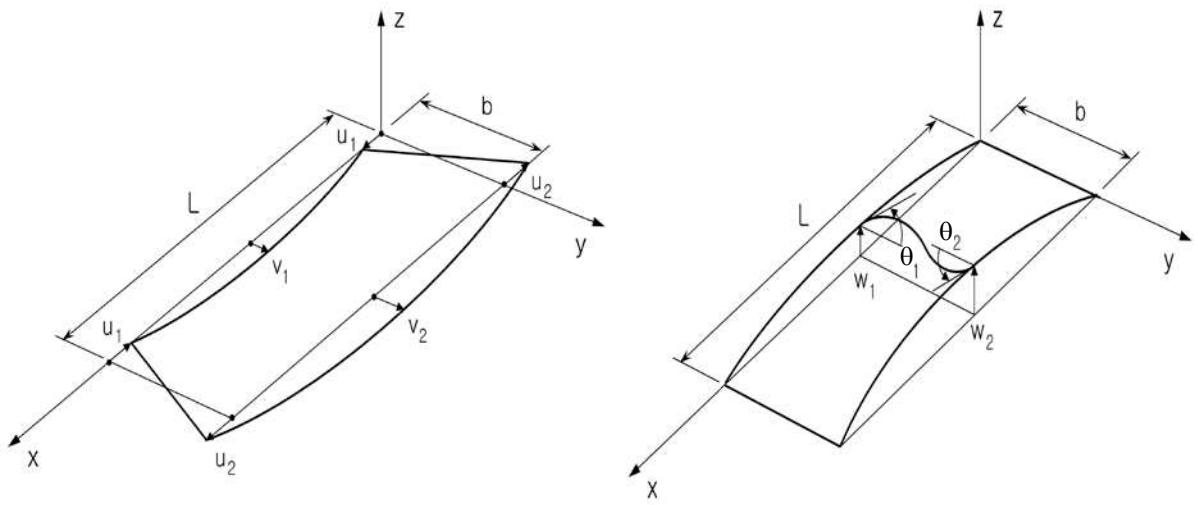


Figure 4: Degrees of freedom of a finite strip

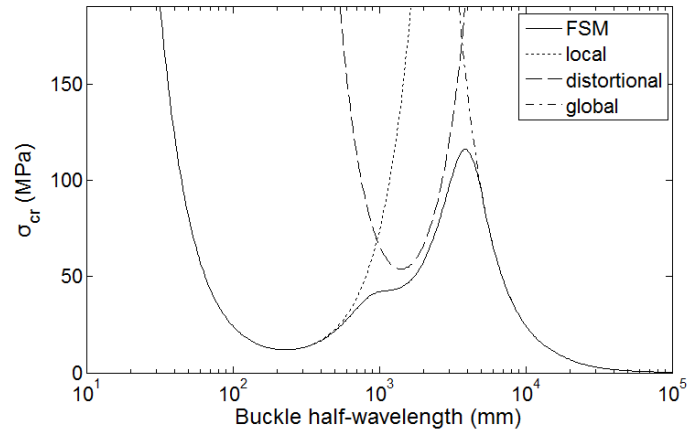


Figure 5: Typical signature curve

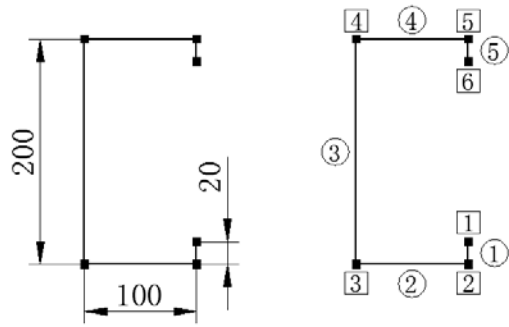


Figure 6: Lipped channel geometry and discretization

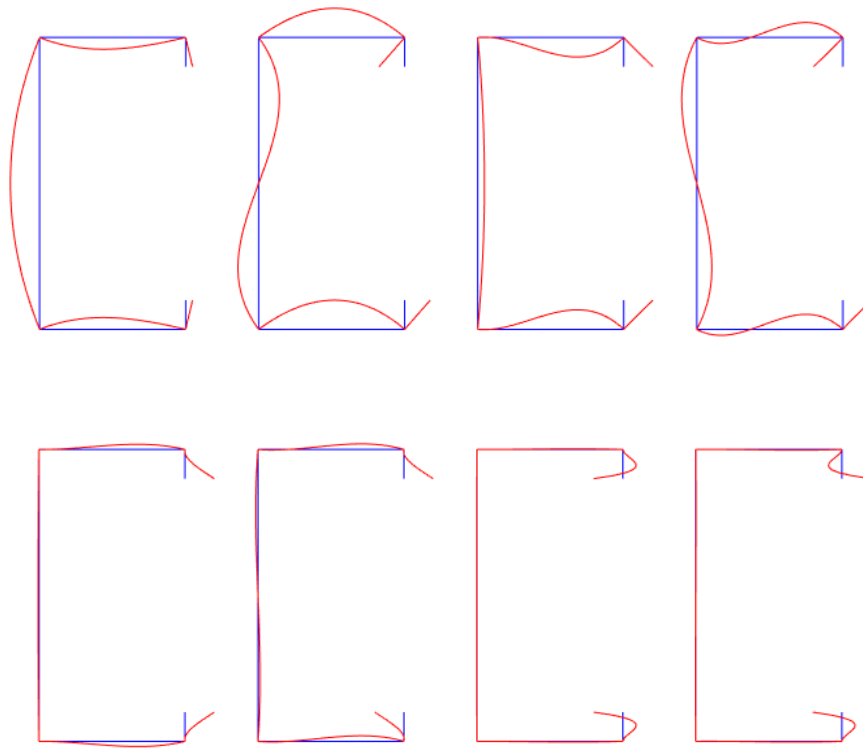


Figure 7: Local buckling modes

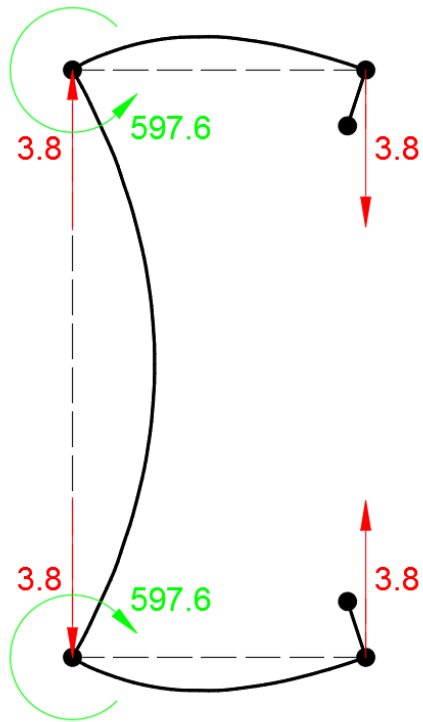


Figure 8: Equivalent nodal forces of the critical local buckling mode (units: N and mm)

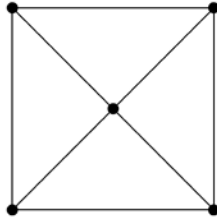


Figure 9: Multi-cell cross-section

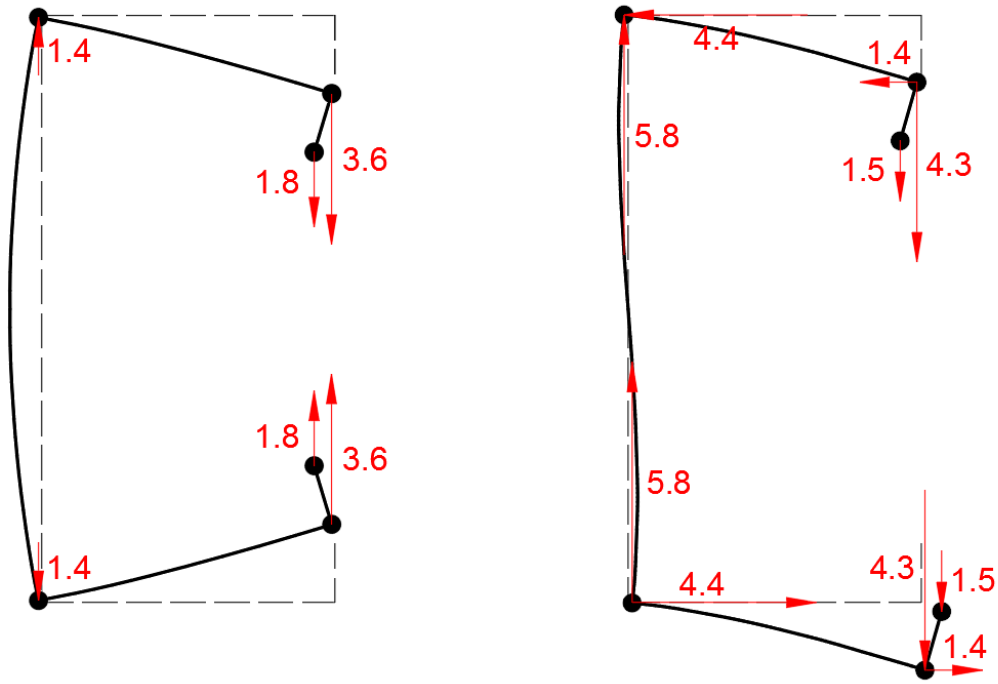


Figure 10: Distortional buckling modes and equivalent nodal forces (unit: N)

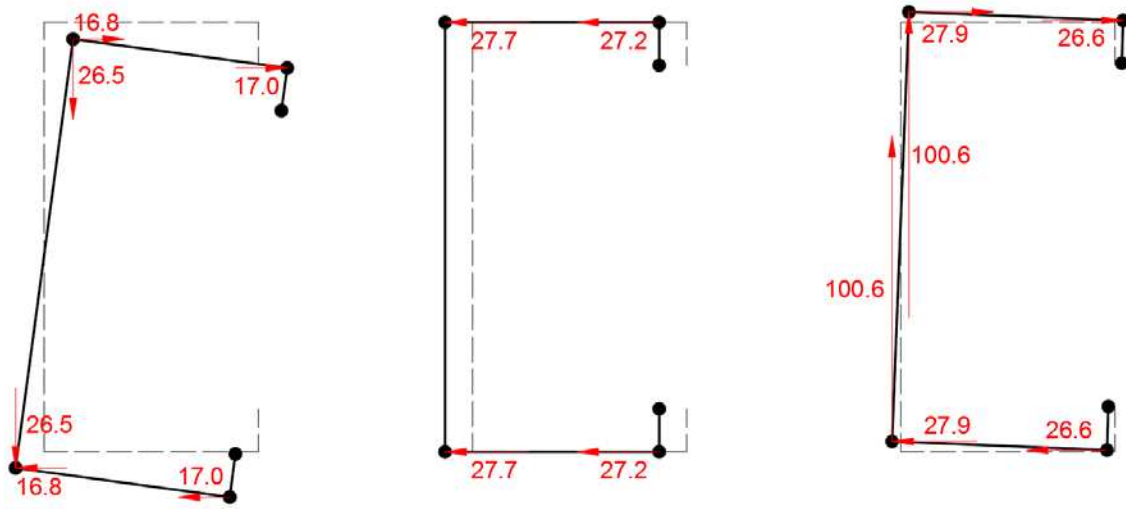


Figure 11: Global buckling modes and equivalent nodal forces (unit: N)

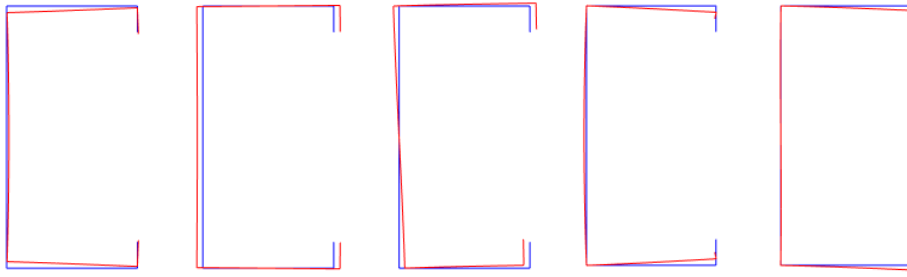


Figure 12: Transverse extension modes

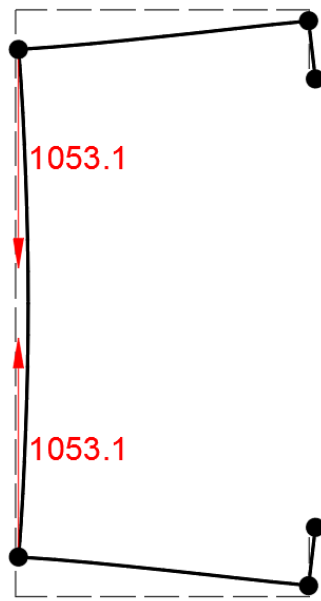


Figure 13: Equivalent nodal forces of the critical transverse extension mode (unit: N)

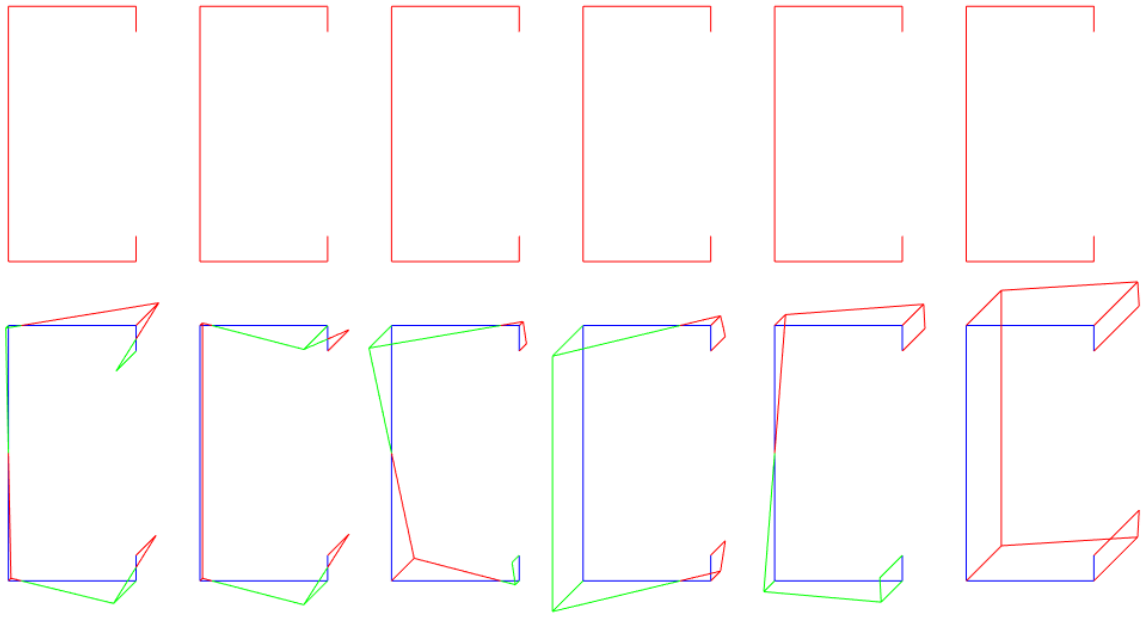


Figure 14: Shear modes: cross-sectional deformations (top) and warping deformations (bottom)

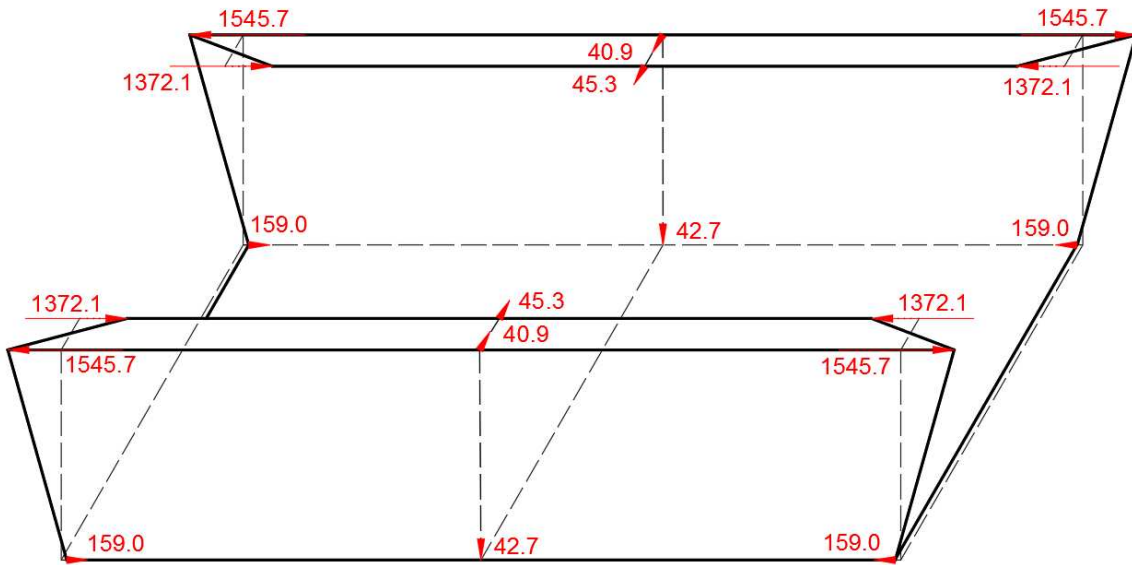


Figure 15: Equivalent nodal forces of a shear mode (unit: N)

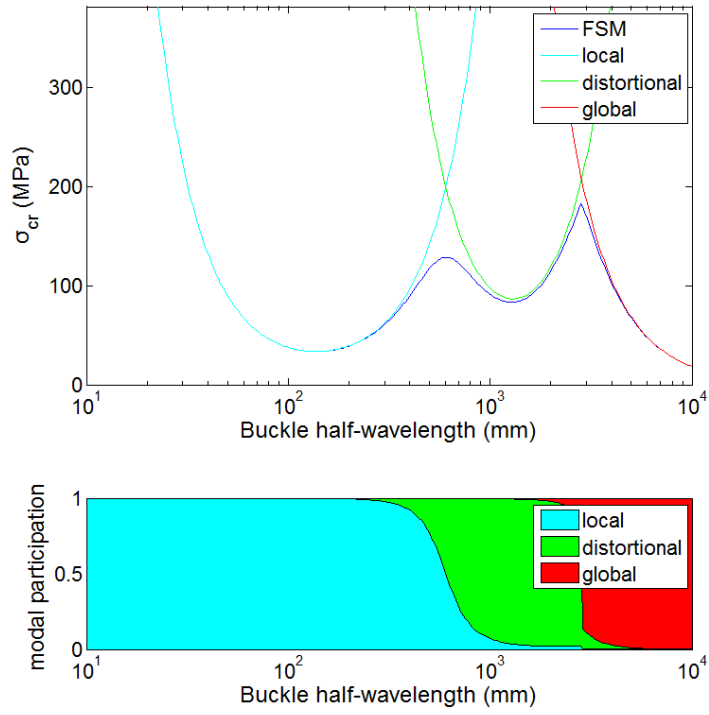


Figure 16: Modal decomposition of the FSM output for the lipped channel in Fig. 6

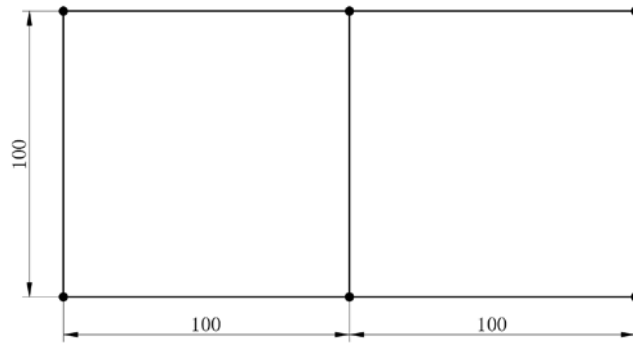


Figure 17: Double-cell cross-section

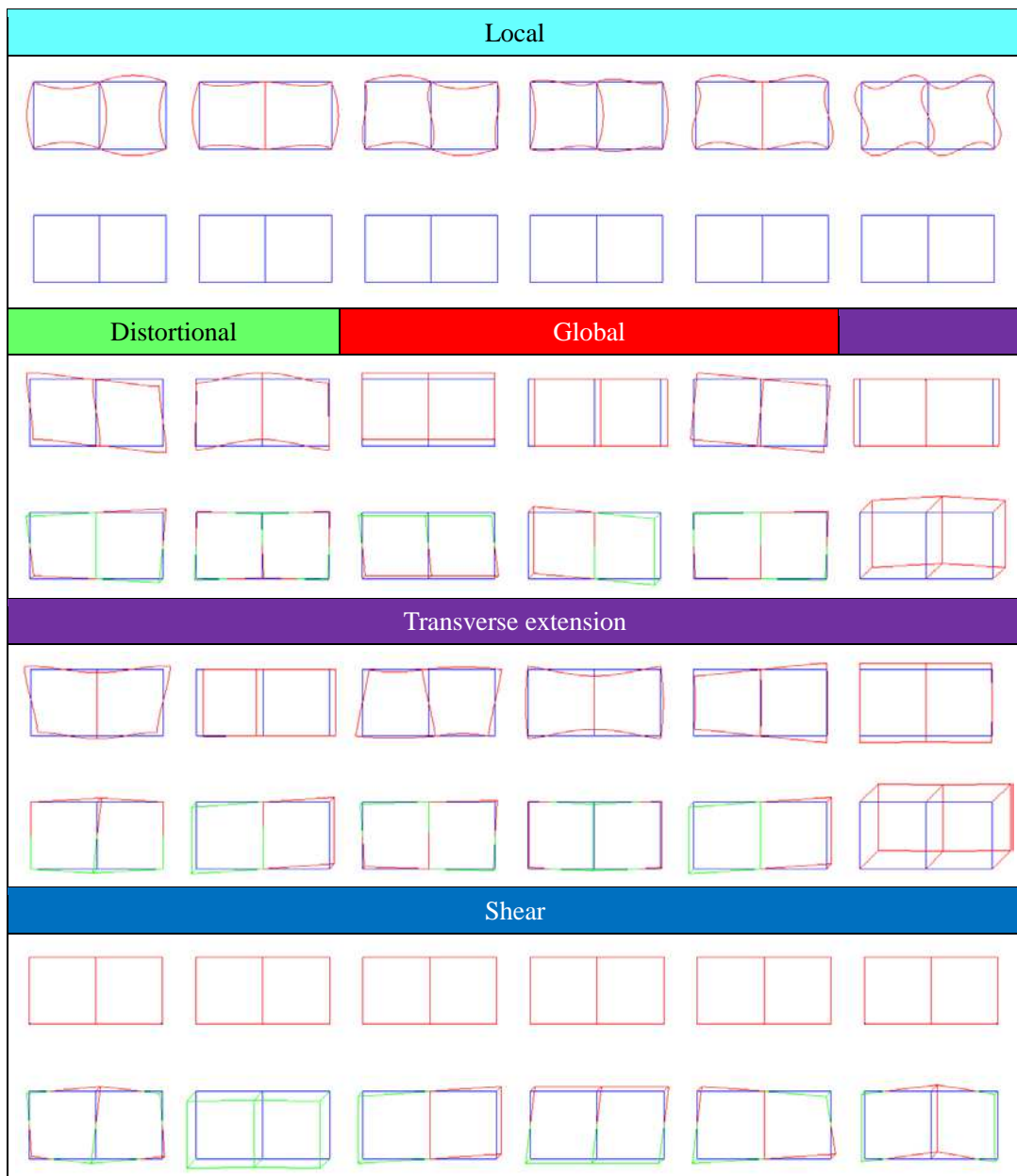


Figure 18: Pure modes of the double-cell cross-section

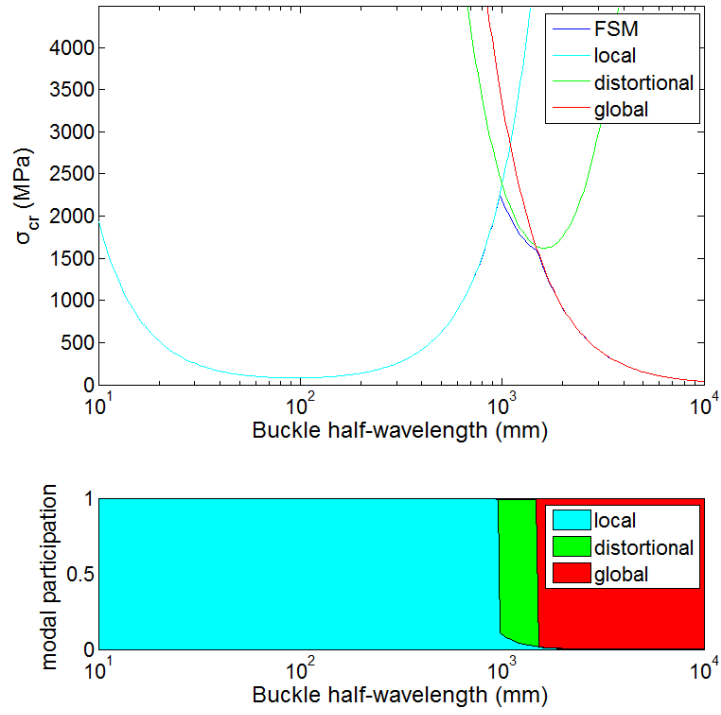


Figure 19: Modal decomposition of the FSM output for the double-cell cross-section

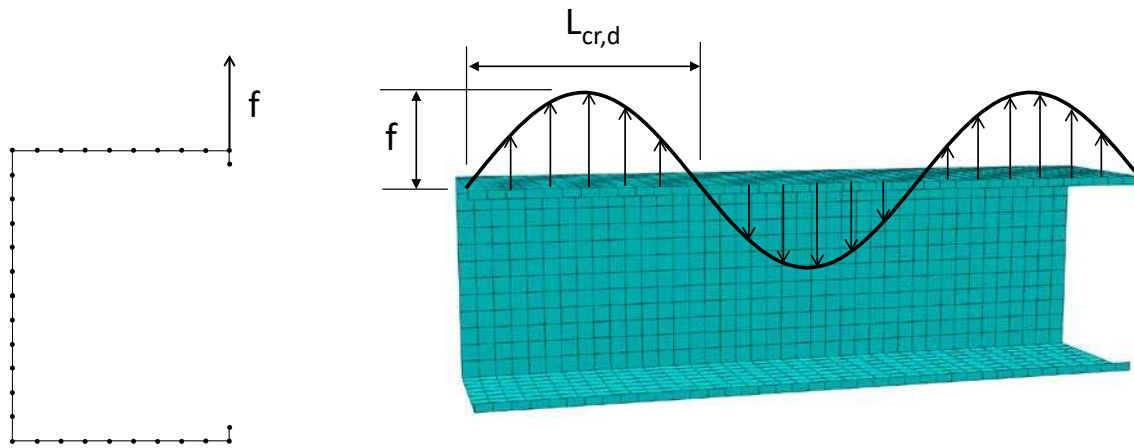


Figure 20: Equivalent line loads in FE applications

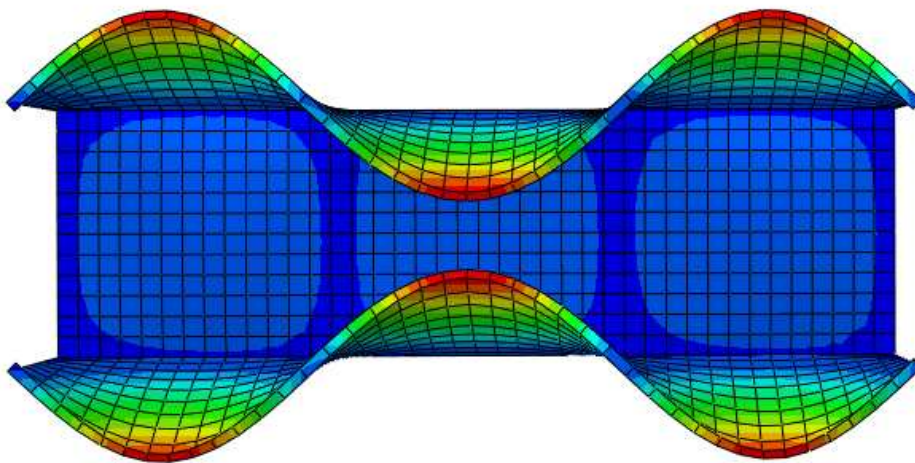


Figure 21: Distortional mode shape generated in FE

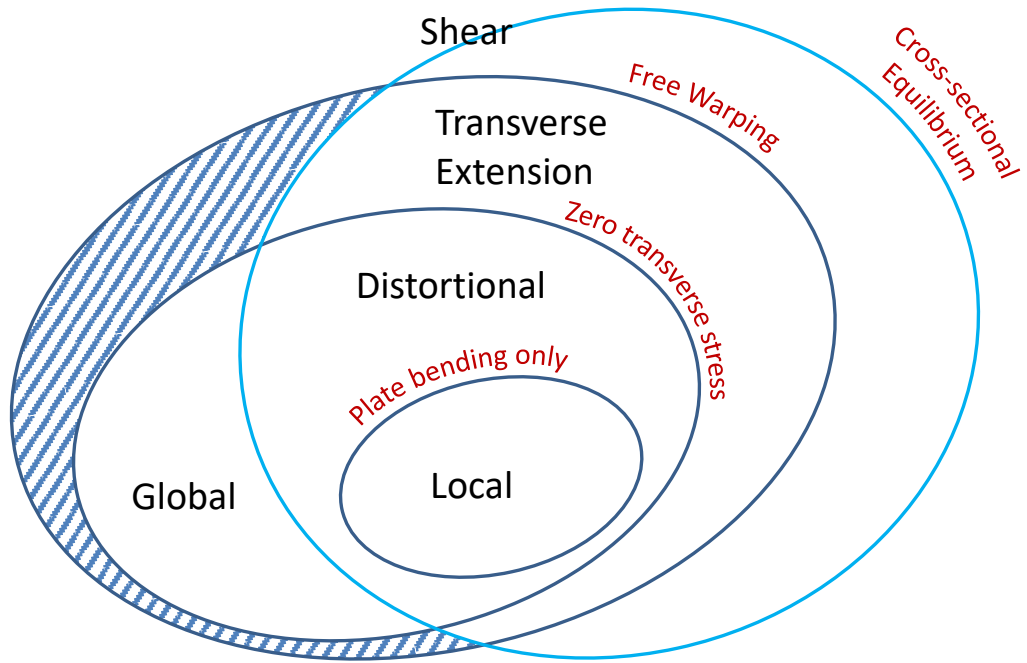


Figure 22: Summary of the mechanical criteria used in the method of the equivalent nodal forces